Spectral-domain, polarization-sensitive optical coherence tomography system insensitive to fiber disturbances

Manuel J. Marques*[a], Sylvain Rivet[a,b], Adrian Bradu[a], Adrian Podoleanu[a]

[a]Applied Optics Group, School of Physical Sciences, University of Kent, Canterbury CT2 7NH, United Kingdom;

[b]Université de Brest, EA 938 Laboratoire de Spectrométrie et Optique Laser, SFR Scinbios, 6 avenue Le Gorgeu, C.S. 93837, 29238 Brest Cedex 3, France

ABSTRACT

This communication presents a spectral-domain, polarization-sensitive optical coherence tomography (PS-OCT) system based on a fiber interferometer using single-mode fibers and couplers. The two orthogonal polarization components which define the polarization state are sequentially detected by a single line camera. Retardance measurements can be affected by polarimetric effects in fibers and couplers. This configuration bypasses such issues by performing the polarization selection before the collection fiber, employing a combination of a polarization rotator and a linear polarizer. Numerical simulations are carried out to verify the tolerance of the proposed configuration to fiber-based disturbances; this was further experimentally verified with similar net retardance maps of a birefringent phantom being obtained for two different settings of induced fiber birefringence.

1. INTRODUCTION

Spectrometer-based optical coherence tomography (OCT) methods have been extensively used over the past decade as a way to image translucent structures.[1] Polarization-sensitive OCT (PS-OCT) methods emerged as early as 1992,[2] evolving from bulk-based to fiber-based designs, employing single or multiple detectors, and acquiring the resulting signal either in time-domain or in frequency-domain.

Fiber-based implementations are useful in the OCT practice due to their robustness and reliability. The configuration presented here belongs to this category. Additionally, a single-camera design is employed for cost-efficiency and simplicity of adjustment. However, external factors (such as temperature and mechanical stress) affect the birefringence of single-mode fibers (SMF) used in OCT systems, inducing disturbances in the measured polarization.

One way of by-passing the issue of the SMF birefringence is to perform the polarization selection before the collecting fiber. Roth *et al*[3] devised such a time-domain, fiber-based system, using a liquid-crystal modulator in the sample arm to vary the polarization state of the light probing the medium according to three polarization states generated sequentially. Fiber-based polarization controllers were used but only to maximize signal amplitude. This approach, however, means that the input polarization state of the light is not circular, which has an impact on the signal-to-noise ratio (SNR) of the images corresponding to the different polarization state settings. Moreover, three measurements have to be performed.

Sample illumination with circularly polarized light was attained in the time-domain, PS-OCT system reported by Al-Qaisi *et al.*,[4] which relied on the modulation of the two orthogonal polarization states in the path delay to multiplex the polarimetric information in one single detector reading. This approach, however, required polarization-maintaining (PM) fibers and couplers to be used, which introduce additional complexity to the system.

In Cense *et al.*[5] a spectral-domain PS-OCT system was implemented using SMFs, which involved a novel spectrometer design employing a Wollaston prism to separate the orthogonal polarization components, projecting them onto different parts of the same detector array. This allows for simultaneous acquisition of the two polarization states; however, it also requires fine tuning of the polarization state of the light within the two arms using fiber-based polarization controllers. Furthermore, projecting the two polarization components onto the same detector array reduces the available number of pixels per component, which will necessarily diminish the axial range attainable with the OCT system, since the spectrometer resolution is reduced.

*mjmm2@kent.ac.uk, phone +44 1227 823288.

Optical Coherence Tomography and Coherence Domain Optical Methods in Biomedicine XX, edited by Joseph A. Izatt, James G. Fujimoto, Valery V. Tuchin, Proc. of SPIE Vol. 9697, 96971K · © 2016 SPIE · CCC code: 1605-7422/16/$18 · doi: 10.1117/12.2213479

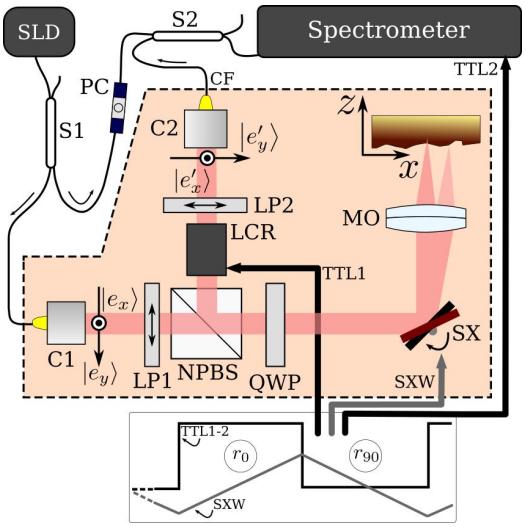

Figure 1. Fiber-based PS-OCT system. SLD: superluminiscent diode; S1-2: fiber-based fused couplers; C1-2: fiber collimators; PC: fiber-based polarization controller; LP1-2: dichroic linear polarizers; NPBS: non-polarizing beam-splitter; QWP: quarter-wave plate (oriented at 45 degrees in respect to the polarization direction selected by LP1); SX: galvo-scanner; MO: microscope objective; CF: collecting fiber; LCR: liquid-crystal polarization rotator switching between states r_0 and r_{90}; SXW: line scanner triangular waveform, each period corresponding to the acquisition of two horizontally-flipped images corresponding to the two states r_0 and r_{90}; TTL1-2: driving signals for the LCR switching and the spectrometer acquisition trigger, respectively. The spectrometer comprises a 1200 l/mm transmissive diffraction grating (Wasatch Photonics, Logan, UT, United States of America) and a CMOS line camera (Basler AG, Ahrensburg, Germany) set at 400 μs line acquisition time.

2. EXPERIMENTAL SET-UP

The configuration presented in this communication operates in spectral-domain and performs the polarization selection before the collecting fiber in a sequential manner. In opposition to Roth *et al.*,[3] the sample is illuminated with circularly polarized light. Since the selection is performed before the collecting fiber, SM fibers and couplers can be used without the requirement of fine-tuning the polarization state, as in Cense *et al.*[5] Unlike Roth *et al.*,[3] the configuration here presented only requires two sequential acquisition steps to obtain the polarimetric measurements from the sample.

The experimental set-up is schematically described in Fig. 1. Light from a superluminiscent diode SLD (Superlum, Moscow, Russian Federation), with central wavelength 830 nm, bandwidth 20 nm, output power ~ 10 mW is split between the two arms of a Mach-Zehnder interferometer at the directional splitter S1, 20% of which is directed to the reference arm and 80% to the sample arm. In the sample arm (shaded region in Fig. 1), a liquid-crystal polarization rotator LCR (Meadowlark LPR-100-800, Frederick, CO, United States of America) is employed to rotate the returned field from the sample between two states, corresponding to no rotation (r_0) and to a 90 degree rotation (r_{90}). Switching between these two states is driven by a TTL signal generated by the computer's DAQ card, shown in Fig. 1 as TTL1. For the two states, the resulting field at the input of the collecting fiber has the same polarization state (linear, along $|e'_y\rangle$) which is selected by the linear polarizer LP2 placed before the fiber. The output field of the fiber is transformed by the polarimetric disturbances of both the fiber CF and the coupler S2. However, this transformation will affect the two rotation states in equal manner; hence, the polarization state of the field leaving the splitter S2 through the spectrometer port is the same for the two rotation states, with only the electric field amplitude varying between them.

The theoretical model[6] describing this system is based on a pure polarization rotator which can be implemented using a LCR as presented in this communication. The amplitude of the modulation resulting from the interference between a scatterer at a depth z and the signal from the reference arm is given by

$$I_{interf} = \begin{cases} |\sin\Phi(z)|\,\Xi = I^{r0} \\ |\cos\Phi(z)|\,\Xi = I^{r90} \end{cases}, \tag{1}$$

where Ξ describes the interference between the fields from the reference and sample arms. This coefficient also takes into account the chromatic response of the fibers. By taking the ratio between these two amplitudes, it is possible to compute the absolute value of the retardance measurement in the medium, $|\Phi|$, given by

$$|\Phi| = \arctan\left[\frac{I^{r0}}{I^{r90}}\right]. \tag{2}$$

After acquisition, the channeled spectra are re-sampled, an inverse Fourier Transform (FT) is performed and the A-scans are bundled together to form a B-scan. The two TTL signals in Fig. 1 are in phase, therefore a 1024-pixel wide B-scan contains two identically-sized B-scan images, corresponding to the two rotation states of LCR, r_0 and r_{90}. The pair of images is refreshed at 2.5 Hz.

3. THEORETICAL SIMULATIONS

Numerical simulations were carried out to verify the behavior presented in the theoretical section, where the retardance measurement of the sample $|\Phi|$ is insensitive to the properties of the collecting fiber CF, which are encoded in the coefficient Ξ . To do so, a sample with its optical axis oriented at 45° and a retardance of 10° is considered, the OCT system is modeled with a Gaussian broadband source ($\lambda_0 = 850$ nm central wavelength, spectral bandwidth $\Delta\lambda = 100$ nm), and the chromaticity of the optical elements within the system is not considered.

The collecting fiber CF and the splitter S2 are modeled by the product J^{Fiber} of a series of Jones matrices, which account for the chromatic birefringence of the fiber and the possible diattenuation of the couplers, as follows:

$$J^{Fiber} = J_{\mathrm{Rot}(\alpha 1)} \cdot J_{\mathrm{Diat}(D,a2)} \cdot J_{\mathrm{Bir}(\phi(\nu),\alpha 3)} \cdot J_{\mathrm{Rot}(\alpha 4)}, \tag{3}$$

where $J_{\mathrm{Rot}(\alpha)}$ is the Jones matrix for a rotator which rotates the linear polarization by an angle α, $J_{\mathrm{Diat}(D,a)}$ corresponds to a linear diattenuator with diattenuation D and oriented at angle α, and $J_{\mathrm{Bir}(\phi(\nu),\alpha)}$ corresponds to a linear retarder oriented at an angle α with retardance $\phi(\nu)$. This retardance is expressed according to a mean retardance $\phi(\nu_0)$ and a parameter ΔT to account for the polarization mode dispersion (PMD) of the fiber, as follows:

$$\phi(\nu) = \phi(\nu_0) + 2\pi\Delta T(\nu - \nu_0), \tag{4}$$

with ν_0 being the central frequency of the optical source.

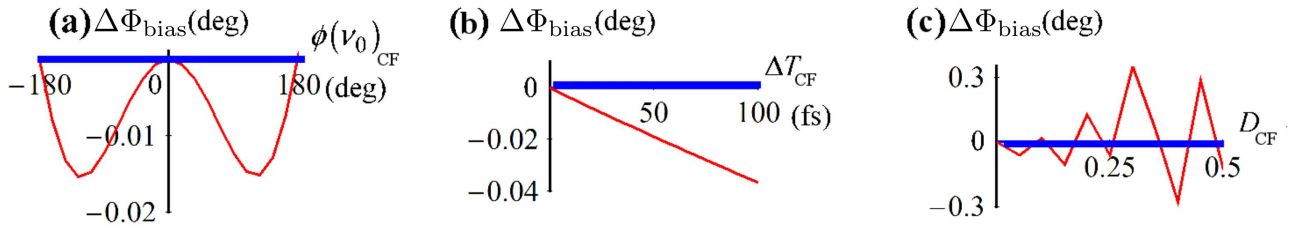

Figure 2. Simulation results for the collecting fiber CF. In (a) the bias on the sample retardance measurement $\Delta\Phi_{\mathrm{bias}}$ is plotted against the CF birefringence (modeled with retardance $\phi(\nu_0)_{\mathrm{CF}}$); in (b) $\Delta\Phi_{\mathrm{bias}}$ is plotted against the PMD ΔT_{CF}; and in (c) $\Delta\Phi_{\mathrm{bias}}$ is plotted against the diattenuation D_{CF}. Thick (blue) lines represent no alteration in the fiber parameters between the two sequential steps of the LCR; thin (red) lines represent a 1% change on the varying parameter between the two sequential steps of the LCR.

In Fig. 2 the bias on the retardance, $\Delta\Phi_{\mathrm{bias}}$ is plotted against the variation on several of the parameters which are present in the collecting fiber model, namely the diattenuation D_{CF}, the mean birefringence $\phi(\nu_0)_{\mathrm{CF}}$ and the PMD ΔT_{CF}. If we consider that the said parameters remain constant during the two sequential steps

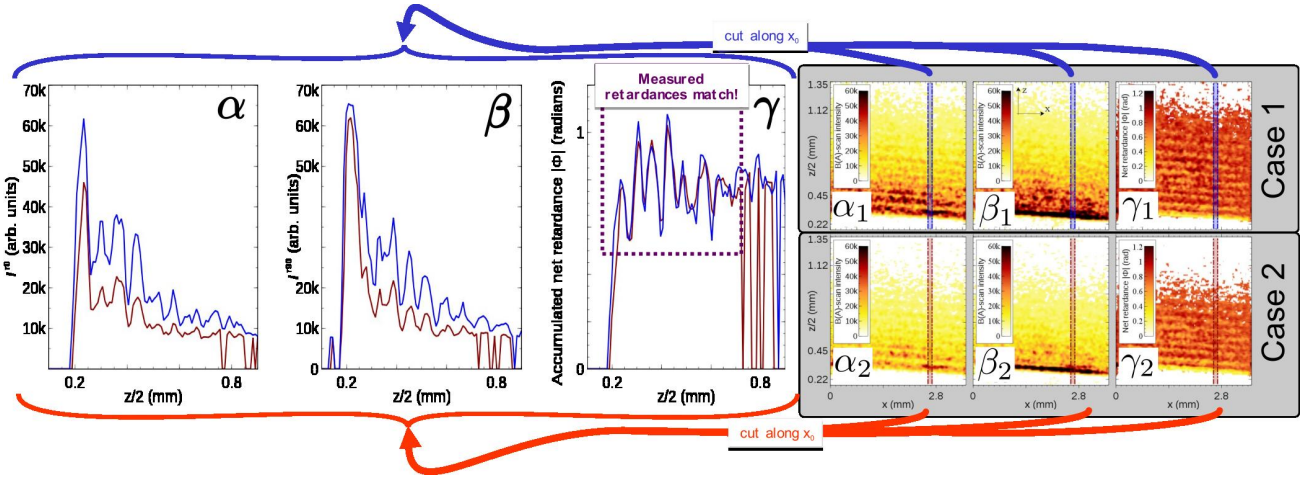

Figure 3. A-scans cut along $x_0 = 2.55$ to 2.65 mm over the B-scans of a plastic phantom exhibiting birefringence (shown in the right panel). Between the top (Case 1) and bottom rows (Case 2) within the panel placed on the right-hand side of the image, the PC settings in the reference arm were adjusted in terms of both pressure on the fiber and rotation to create different fiber-induced polarization states and simulate in this way polarization disturbances.

of the LCR, as is the case with all three thick (blue) curves, the bias in the measurement is equal to zero. If, however, there is a small change (1% of the previous value) on the parameters, a nonzero bias arises, as shown in the thin (red) curves in Fig. 2. This bias is quite weak (<1%), hence the device would still perform with adequate accuracy even if the fibers are disturbed during the measurements, at a rate comparable to the switching rate of the LCR.

4. RESULTS

To demonstrate the insensitivity of the system to the perturbations caused by the collecting fiber, two sets of images were generated (Cases 1 and 2). Between them, the polarization controller PC on the reference arm was adjusted to mimic such perturbations. Both are represented in Fig. 3 , with frames α_1, α_2 depicting the 2-D maps for the state r_0, β_1, β_2 the 2-D maps for r_{90}, and γ_1, γ_2 the net retardance maps $|\Phi|$ resulting from the ratio I^{r0}/I^{r90} (Eq. (2)). The lateral size in all images is 3.5 mm, and the usable range in depth is ~ 1.6 mm.

It is clear from comparing the two pairs of 2-D maps (α_1 vs α_2, β_1 vs β_2) that the maps corresponding to Case 2 have a different contrast from those of Case 1, as a result of the polarization disturbances which introduce a mismatch between the polarization states of the two arms of the interferometer, lowering the interferometric modulation. Even so, the resulting retardance maps γ_1 and γ_2 show similar levels of birefringence, despite the perturbation introduced by the fiber. This is further verified in the graphs α, β, γ shown on the left-hand side of Fig. 3, where A-scans along $x_0 = 2.55$ to 2.65 mm are represented for all the 6 frames in Fig. 3 after some lateral averaging has been carried out within the area between the vertical dashed lines.

5. CONCLUSIONS

In order to measure solely the net retardance, a polarization-sensitive spectral-domain OCT system using a broadband source and a spectrometer has been demonstrated. The system does not require compensation methods and is insensitive to the fiber-induced birefringence, provided it does not vary with a rate similar to that of the switching device. The sample is illuminated with circularly polarized light, which improves the efficiency of the retardance measurements in case the sample is a linear retarder. Due to its single-detector architecture, this system requires two measurements to be performed sequentially, while securing in this way the axial range allowed by the entire detector array during each measurement. For this proof of concept, a liquid-crystal device was employed as a polarization rotator, with some limitations in terms of acquisition speed.

ACKNOWLEDGMENTS

M. J. Marques, A. Bradu and A. Podoleanu were partially supported by the European Research Council (ERC) under the European Union's Seventh Framework Programme, Advanced Grant agreement "COGATIMABIO", grant no. 249889. A. Podoleanu is also supported by the European Industrial Doctorate UBAPHODESA, FP7-PEOPLE-2013-ITN 607627 and by the NIHR Biomedical Research Centre at Moorfields Eye Hospital NHS Foundation Trust and UCL Institute of Ophthalmology. S. Rivet acknowledges the Marie-Curie Intra-European Fellowship for Career Development, no. 625509. M. J. Marques also acknowledges the University of Kent for his PhD support.

REFERENCES

1. W. Drexler, M. Liu, A. Kumar, T. Kamali, A. Unterhuber, and R. A. Leitgeb, "Optical coherence tomography today: speed, contrast, and multimodality.," *J. Biomed. Opt.* **19**, p. 71412, jul 2014.
2. M. R. Hee, D. Huang, E. A. Swanson, and J. G. Fujimoto, "Polarization-sensitive low-coherence reflectometer for birefringence characterization and ranging," *J. Opt. Soc. Am. B* **9**, p. 903, jun 1992.
3. J. E. Roth, J. A. Kozak, S. Yazdanfar, A. M. Rollins, and J. A. Izatt, "Simplified method for polarization-sensitive optical coherence tomography," *Opt. Lett.* **26**, p. 1069, jul 2001.
4. M. K. Al-Qaisi and T. Akkin, "Polarization-sensitive optical coherence tomography based on polarization-maintaining fibers and frequency multiplexing.," *Opt. Express* **16**(17), pp. 13032–13041, 2008.
5. B. Cense, M. Mujat, T. C. Chen, B. H. Park, and J. F. de Boer, "Polarization-sensitive spectral-domain optical coherence tomography using a single line scan camera.," *Opt. Express* **15**(5), pp. 2421–31, 2007.
6. M. J. Marques, S. Rivet, A. Bradu, and A. Podoleanu, "Polarization-sensitive optical coherence tomography system tolerant to fiber disturbances using a line camera," *Opt. Lett.* **40**(16), pp. 3858–3861, 2015.